Electronic Supplementary Material (ESI) for Journal of Materials Chemistry A.

Supporting Information for

Facile synthesis of Fe^{3+}/Fe^{2+} self-doped nanoporous $FeVO_4$ photoanodes for efficient solar water splitting

Wei Wang,[a,b] Yajun Zhang,[a] Lei Wang[a] and Yingpu Bi[a,*]

[a] State Key Laboratory for Oxo Synthesis & Selective Oxidation, National Engineering Research Center for Fine Petrochemical Intermediates Lanzhou Institute of Chemical Physics, CAS, Lanzhou, Gansu 730000 (P.R. China). E-mail: yingpubi@licp.cas.cn

[b] University of Chinese Academy of Sciences, Beijing 100049, China.

Experimental

1. Materials

Iron (III) nitrate nonahydrate ($Fe(NO_3)_3{\cdot}9H_2O$, 98.5%), ammonium metavanadate (NH_4VO_3, 99.0%), citric acid anhydrous ($C_6H_8O_7$, 99.0%), polyethylene glycol 600 (PEG-600, 99.5%), sodium borohydride ($NaBH_4$, 96.0%), hydrogen peroxide (H_2O_2, 30%), ethanol (CH_3CH_2OH, 99.7%), ammonium ferrous sulfate hexahydrate ($Fe(NH_4)_2(SO_4)_2{\cdot}6H_2O$, 99.5%), *o*-phenanthroline ($C_{12}H_8N_2{\cdot}H_2O$, 99.0%), hydroxylamine hydrochloride ($H_2NOH{\cdot}HCl$ 98.5%), sodium acetate (CH_3COONa, 99.0%) and (CH_3COOH, 99.5%) were purchased from Sinopharm Chemical Reagent Co. Ltd (AR quality) and were utilized without further purification. Deionized water (18 MV, Molecular) was used for all solution preparations. FTO (1.0×5.0 cm^2)-coated glass slides were thoroughly cleaned via sonication in successive solutions of acetone, isopropanol, ethanol, and finally rinsed with Deionized water. All illuminated areas were 1 cm^2.

2. Synthesis

$FeVO_4$ was synthesized using $Fe(NO_3)_3{\cdot}9H_2O$ and NH_4VO_3 and $C_6H_8O_7$. The 1.5 mmol $Fe(NO_3)_3{\cdot}9H_2O$ and 0.5 mmol $C_6H_8O_7$ were dissolved in 20 ml distilled water and stirred at 80 °C for 5 min to enhance complete dissolution. A 1.5 mmol NH_4VO_3 was dissolved similarly (~80 °C, <5 min). Then, NH_4VO_3 was added into the $Fe(NO_3)_3{\cdot}9H_2O$ solution, and the mixtures were kept at 80 °C for 30 min, which quickly formed a yellow nanoparticle colloid ($FeVO_4$-membrane). Next, 0.12 g of PEG-600 was dissolved in 10 mL ethanol and then transferred to the solution of $FeVO_4$ to enhance wetting and uniformity of the coating. The solution was agitated by shaking for 1.0 h at room temperature until it became completely reaction, and the colloid became significantly more yellow. This solution of $FeVO_4$ was noted for $FeVO_4$-nanoporous. Further, the resulting $FeVO_4$-nanoporous suspension was centrifuged, washed with ethanol and water before being dried in an oven at 80 °C to obtain an orange-brown solid ($FeVO_4$-nanoparticles).

Next, we used this three distinct types of $FeVO_4$ precursor solution (200 μL) drop-cast on FTO substrates that had been cleaned previously. The samples were dried in an oven at 80 °C for 55 min and then annealed in air at 500 °C for 2.5 hours, a yellow/orange film was obtained on the FTO substrates. The molar ratio of the NH_4VO_3 and $Fe(NO_3)_3{\cdot}9H_2O$ was kept at 1:1 in all

experimental conditions. For comparison, the $FeVO_4$-nanoprous films were synthesized via adjusting the synthesis conditions, such as the annealing temperature and annealing time for the precursor solution. All films had the same mass of active material, so that the effects of size and morphology could be observed.

The Fe^{3+} self-doped $FeVO_4$-nanoprous films were obtained using oxidation method by immersing $FeVO_4$-nanoprous films into H_2O_2 (30 wt %) for 10 min. Then, the films were washed with water, and dried under nitrogen. Meanwhile, a reduction method was used to obtain the Fe^{2+} self-doping $FeVO_4$ film, which was immersing the $FeVO_4$-nanoprous films into freshly made $NaBH_4$ solution (0.2 mol L^{-1}) for 1 min. Then, the prepared films were washed with water, and dried under nitrogen.

3. Materials characterization

The morphology and size of the as-prepared products were characterized by using a field-emission scanning electron microscope (FE-SEM, JSM-6701F, JEOL) operated at an accelerating voltage of 5 kV. Transmission electron microscopy (TEM) measurements were carried out by using a FEI Tecnai TF20 microscope operated at 200 kV. The X-ray diffraction spectra (XRD) measurements were performed on a PANalytical X'Pert PRO instrument using Cu Kα radiation (40 kV). The XRD patterns were recorded from 10° to 60° with a scanning rate of 0.067°/s. UV-visible diffuse reflectance spectra (UV-vis DRS) were taken on a UV-2550 (Shimadzu) spectrometer by using $BaSO_4$ as the reference. The element composition was detected by X-ray photoelectron spectroscope (XPS, ESCALAB 250Xi). Infrared spectra were recorded from pressed KBr discs on a Nexus 870 spectrometer (IR, Nicolet).

4. Electrochemical and PEC measurements

The electrochemical and PEC measurements were conducted using a three-electrode electrochemical cell with the different $FeVO_4$ films as the working electrode, Ag/AgCl (3 mol L^{-1} KCl) as the reference electrode and platinum sheet as the counter electrode. Unless explicitly noted, all the PEC characterizations were conducted using back illumination in this study. An electrochemical workstation (CH Instruments 760E) was employed for the electrochemical measurements.

The measured potential vs. the Ag/AgCl (3 mol L^{-1} KCl) reference electrode was converted to the reversible hydrogen electrode (RHE) scale via the Nernst equation:

$$E_{RHE} = E_{Ag/AgCl} + 0.0591 \times pH + E_{Ag/AgCl(3\,mol\,L^{-1}\,KCl)}$$

where $E_{Ag/AgCl\ (1\ M\ KCl)}$ =0.222 V at 25 °C, where pH is a pH value of the electrolyte.

A Newport 150 W solar simulator with an air mass 1.5 (AM 1.5G, 100 mW cm^{-2}) filter was used as the illumination source. The light intensity was calibrated to 100 mW cm^{-2} using a thermopile detector (Newport, Models 1916C and 818-P).

The incident photon to current efficiency (IPCE) was determined using a full solar simulator (Newport, Model 9600, 300W Xe arc lamp) and a motorized monochromator (Oriel Cornerstone130 1/8 m). IPCE was measured at 1.0 V vs. Ag/AgCl in 0.2 mol L^{-1} Na_2SO_4 and 0.1 mol L^{-1} phosphate buffer (pH=7) using the same three-electrode system described above for photocurrent measurements. IPCE values was calculated as follows:

A monochromator (Photon Technology International), silicon photodetector (model 818-UV, Newport)

$$IPCE(\%) = \frac{1240 \times I(mA/cm^2)}{P_{light}(mW/cm^2) \times \lambda(nm)} \times 100$$

Where I is the measured photocurrent density at a specific wavelength, λ is the wavelength of incident light and P_{light} is the measured light power density at that wavelength.

The electrochemical impedance spectroscopy (EIS) were obtained at open circuit potential (vs. Ag/AgCl) with small AC amplitude of 5 mV in the frequency range of 10^{-2} to 10^{5} Hz. The measured spectra were fitted with Z view.

5. Photoelectrochemical H_2 and O_2 evolution

Detection of H_2 and O_2 evolution were performed in a three-electrode cell in a self-made photoreactor, in which the photoanode and the counter electrode were separated by an Amberplex membrane. A detailed experimental setup was shown in Fig. S9. A 70 mL of 0.2 mol L^{-1} Na_2SO_4 and 0.1 mol L^{-1} phosphate buffer (pH=7) on either side of the half reaction compartments

were utilized as electrolyte, a $FeVO_4$ films and Pt wire were used as photoanode and photocathode, respectively, Ag/AgCl (3 mol L^{-1} KCl) was used as reference electrode. An illumination intensity of AM 1.5G, 100 mW cm^{-2} filter and a bias of 0.8 V (vs. Ag/AgCl) were used to ensure a better signal-to-noise ratio. According to the standard H_2 and O_2 evolution curve, the amount of generated H_2 was measured by taking 50 µL of gas from the headspace of the cell using a syringe and injecting it into the gas-sampling loop of the GC every 20 min.

Faradaic efficiency (F.E.) was calculated based on the following equation: F.E. [%] = (moles of the product produced for the time duration) × (number of electrons to produce one molecule of the product via water splitting) × 100% / (moles of electrons passing through the cell for the time duration)[1].

6. Synchronous illumination XPS experiments

System diagram of the Synchronous illumination X-ray photoelectron spectroscopy (SIXPS) was shown in Fig. 2A. Different from the normal XPS, a Newport 150 W solar simulator with an air mass 1.5 (AM 1.5 G, 100 mW cm^{-2}) filter was used as illumination source. In the process of measurements, the changes of XPS spectra were recorded by controlling light on or off at given time intervals.

7. Light scattering

Optical system diagram of the monochromatic light scattering has been shown in Fig. S9. The illumination source is also a 300 W Xe arc lamp. The wavelength of incident light was adjusted by a motorized monochromator (Oriel Cornerstone 130 1/8 m).

8. Determination of Fe^{2+} and Fe^{3+}

A *o*-phenanthroline colorimetric method was used for the determination of Fe^{2+} and Fe^{3+} concentrations in the doped and un-doped $FeVO_4$-nanoporous samples[2, 3]. Fe^{2+} was quantified by determining the colored complex Fe^{2+}-phenanthroline at 510 nm. Fe^{3+} was also quantified by subtracting the Fe^{2+} concentration from the total Fe concentration. The total Fe concentration was determined by measuring the Fe^{2+} concentration after Fe^{3+} was reduced by $H_2NOH{\cdot}HCl$. The volume and concentration of $H_2NOH{\cdot}HCl$ used to reduce the Fe^{3+} were 1 mL and 10%, respectively.

For absorbance measurements, a UV-visible light spectrophotometer (TU-1980, Beijing Purkinje General Instrument Co., Ltd) was used. The pH of the solution was adjusted using sulfuric acid or sodium hydroxide, and then pH measurements were made with a Mettler Toledo pH meter (Switzerland) calibrated with acidic standard buffers ranging from pH 4.0-6.86 (25 ^{o}C).

Solutions for iron calibration were obtained by placing in colorimetric tube (50 mL), the standard solution of 0.01mg/mL $Fe(NH_4)_2(SO_4)_2 \cdot 6H_2O$, desired volume of 0-10 mL, and water up to an approximate total volume of 25 mL; this mixture was adjusted until a pH value of 3.5 was reached. Then each additions were mixed in the above mixtures, 1 mL of 10 % $H_2NOH \cdot HCl$, 5mL of sodium acetate buffer, 2 mL of 0.15 % *o*-phenanthroline, and water up to the mark. After 15 min, the developed color was measured against water blank at 510 nm, correcting the signal by subtracting the absorbance value at 700 nm.

Solution for the test sample were obtained by placing one prepared $FeVO_4$ film in small Erlenmeyer flasks and adding 20 mL H_2SO_4 (0.2 mol L^{-1}) with ultrasonic 20 min to enhance complete dissolution. The desired volume of sample solutions were in duplicate, watered up to 50 mL, and adjusted pH = 3.5. The resulting mixture was heated during 10 min in order to avoid interferences in the iron determination. As the solution cooled, then transferred into the colorimetric tube (50 mL), and watered up to an approximate total volume of 25 mL, respectively. For iron determination in the resulting sample solutions, the same procedures described for the calibration solutions were applied.

Additional figures and discussions

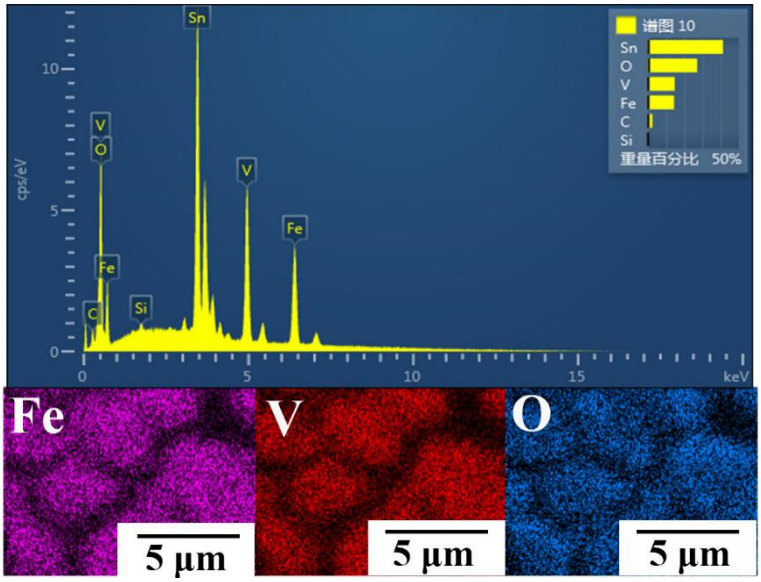

Fig. S1 EDS images and elemental mapping of $FeVO_4$-nanoporous photoanode annealed at 500 °C for 2.5 h.

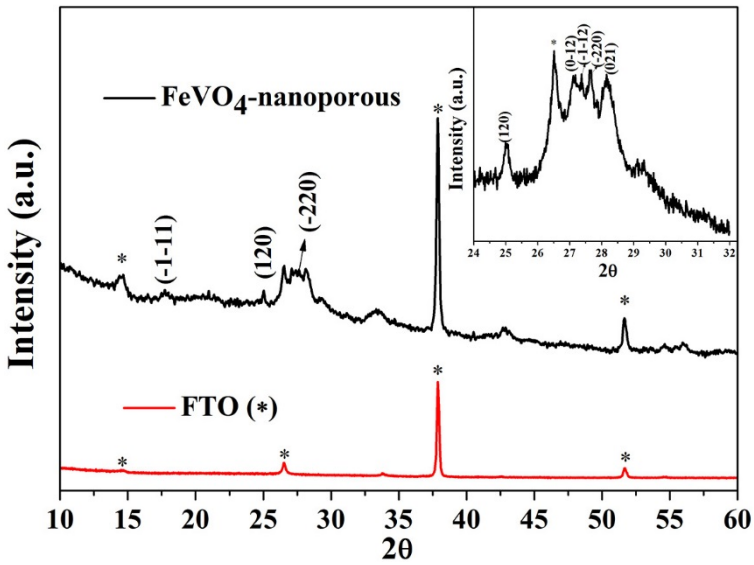

Fig. S2 The XRD patterns of $FeVO_4$-nanoporous photoanode annealed at 500 °C for 2.5 h.

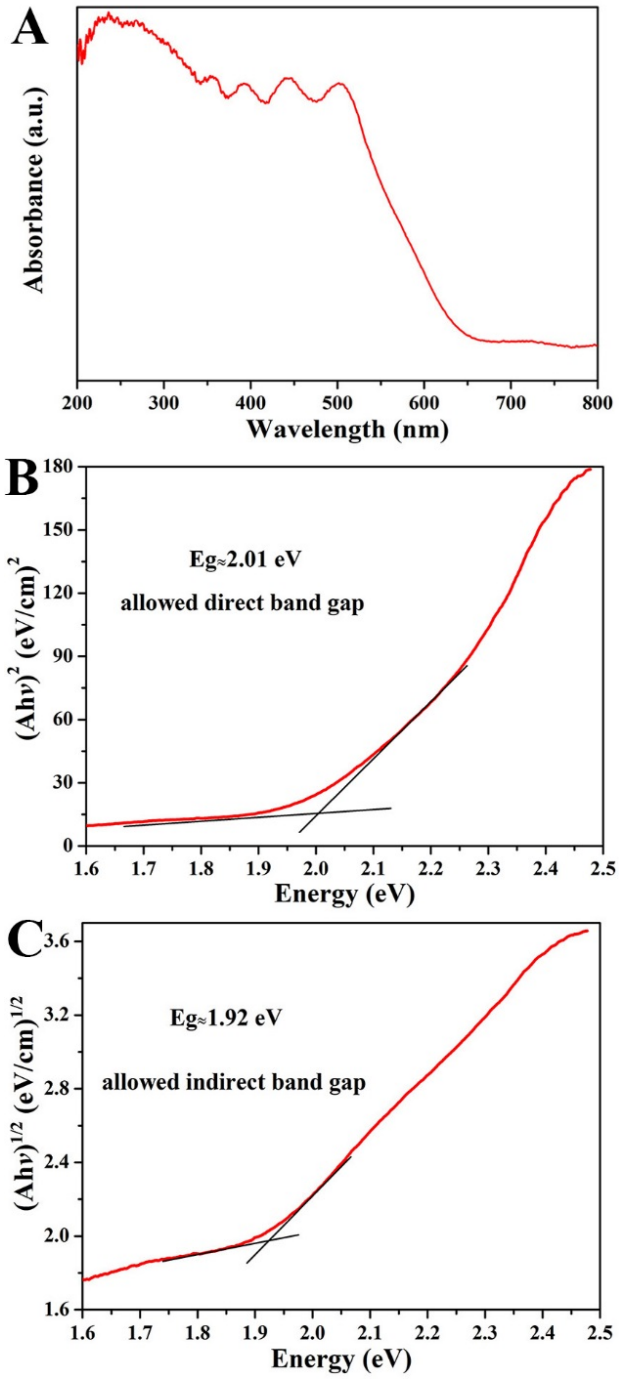

Fig. S3 (A) Absorbance spectrum of $FeVO_4$-nanoporous photoanode annealed at 500 °C for 2.5 h, and (B) the derived Tauc plots corresponding to allowed direct or (C) allowed indirect transitions. The absorption edge of the $FeVO_4$-nanoprous photoanode extends to the visible-light region (around 650 nm), and the bandgap of the $FeVO_4$-nanoporous film is estimated to be ～1.92 to 2.01 eV.

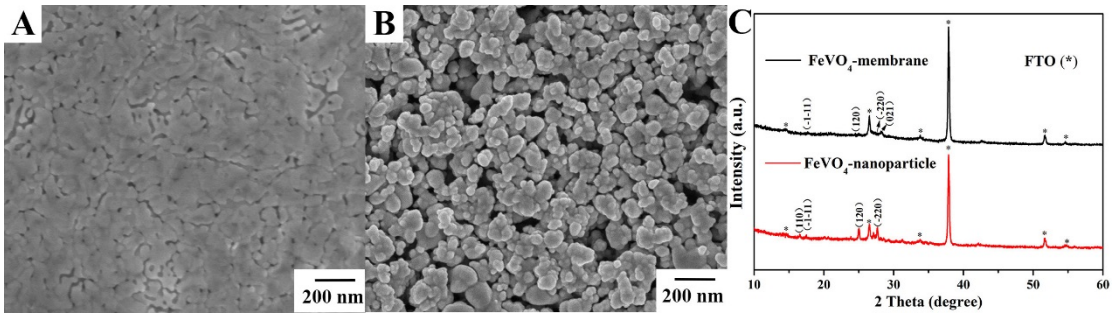

Fig. S4 FE-SEM images of (A) $FeVO_4$-membrane, (B) $FeVO_4$-nanoparticles photoanodes annealed at 500 °C for 2.5 h, and (C) XRD patterns of $FeVO_4$-membrane and $FeVO_4$-nanoparticles. The characteristic peaks of XRD patterns could be indexed to the orthorhombic phase $FeVO_4$ (JCPDS, No. 038-1372). From the sharp and well defined peaks, $FeVO_4$-nanoparticles have a well crystalline nature compared with $FeVO_4$-membrane.

Table S1. Surface area of different $FeVO_4$ structures obtained from N_2 adsorption-desorption measurement. The measurement were conducted using powder samples that were scraped from the films. The nanoporous structure exhibits higher BET surface area compared with membrane and nanoparticle, which leads to substantially more effective photocatalytic performance.

samples	S_{BET} ($m^2\ g^{-1}$)
$FeVO_4$-membrane	18.9641
$FeVO_4$-nanoporous	32.0355
$FeVO_4$-nanoparticle	22.5499

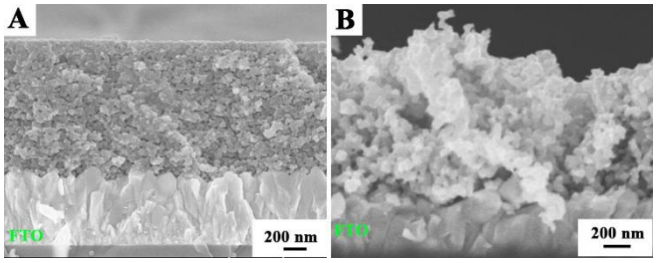

Fig. S5 The cross section of FE-SEM images of (A) $FeVO_4$-membrane and $FeVO_4$-nanoparticles. The thickness of covering $FeVO_4$ layers are about 1.0 µm.

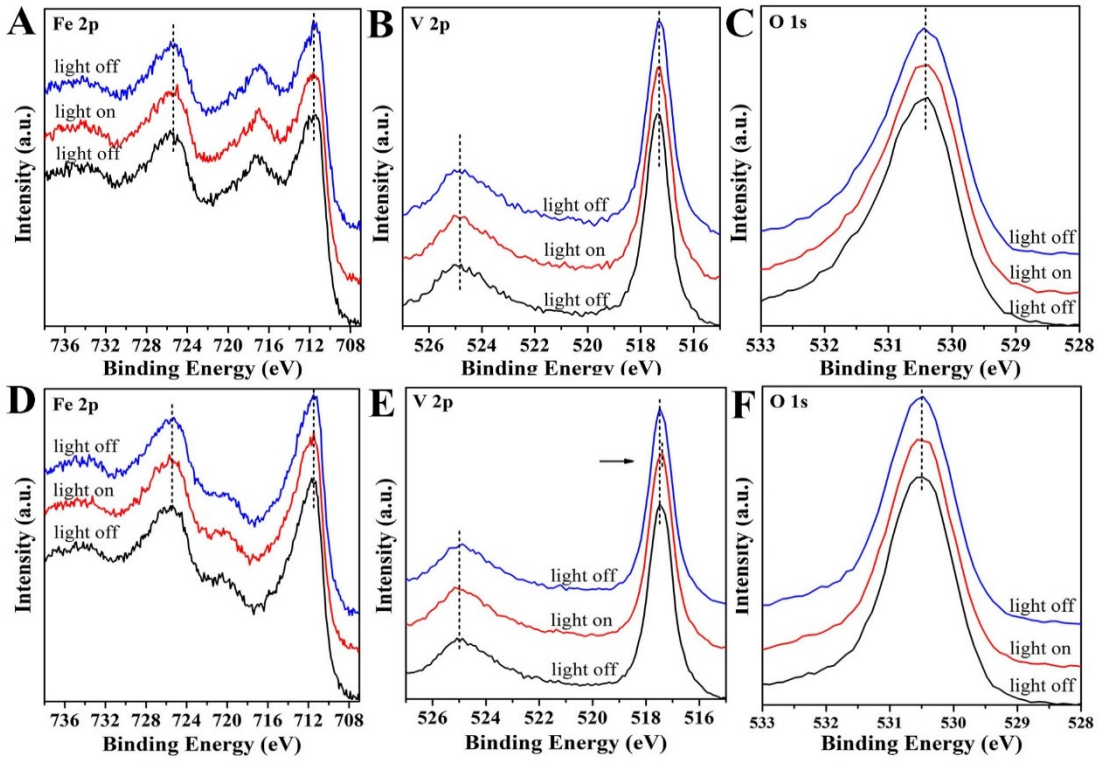

Fig. S6 The SIXPS spectra for Fe 2p, V 2p and O 1s of (A-C) $FeVO_4$-membrane photoanode and (D-F) $FeVO_4$-nanoparticles photoanode, respectively.

Table S2. Fitting results of Nyquist plot in Fig. 3.

Samples	Rs(Ω)/r(%)	CPE-T(F)/r(%)	CPE-P(F)/r(%)	Rct(Ω)/r(%)
$FeVO_4$-membrane	99.98/0.99	3.05×10^{-4}/1.31	0.72/0.65	26669/5.65

$FeVO_4$-nanoporous	75.55/0.63	1.38×10^{-3}/0.91	0.87/0.53	12687/5.30
$FeVO_4$-nanopaticle	282.8/0.50	1.52×10^{-3}/0.85	0.87/0.59	19677/6.77
Fe^{3+} self-doped $FeVO_4$-nanoporous	106.00/0.59	1.29×10^{-3}/1.01	0.85/0.63	4759/2.73
Fe^{2+} self-doped $FeVO_4$-nanoporous	84.84/1.05	1.11×10^{-3}/2.33	0.83/1.28	1657/2.97

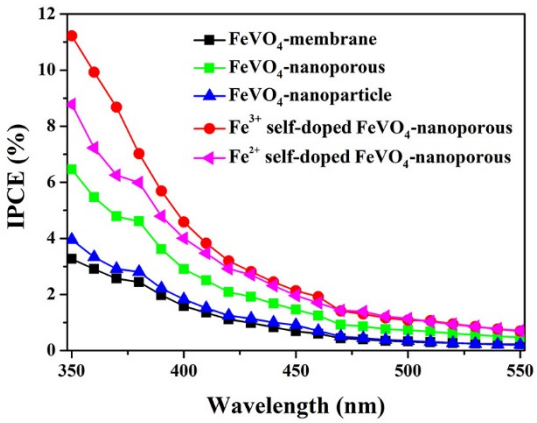

Fig. S7 The IPCE of the $FeVO_4$-membrane, $FeVO_4$-nanoprou, $FeVO_4$-nanoparticles, Fe^{3+} self-doped $FeVO_4$-nanoporous and Fe^{2+} self-doped $FeVO_4$-nanoporous photoanodes in electrolyte of 0.2 mol L^{-1} Na_2SO_4 and 0.1 mol L^{-1} phosphate buffer solution (pH 7.0).

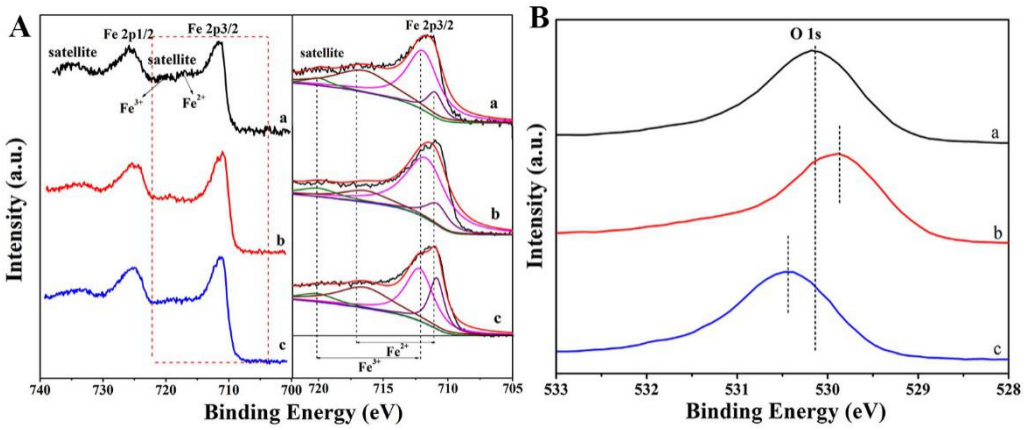

Fig. S8 The XPS spectra of (a) $FeVO_4$-nanoporous, (b) Fe^{3+} self-doped $FeVO_4$-nanoporous and (c) Fe^{2+} self-doped $FeVO_4$-nanoporous photoanodes: the core-level peaks of (A) Fe 2p and (B) O 1s. As shown in the core-level peaks of Fe, the satellite peak obtains at 717.1 eV, which indicates Fe^{2+} exists in the lattice of $FeVO_4$-nanoporous[4]. The Fe^{2+} and Fe^{3+} ions were assumed to generate overlapping Fe 3p spectra[4]. These peaks could be fitted into two peaks to obtain the Fe^{2+} and Fe^{3+} ratios[4]. Generally, the relative areas changes of Fe^{3+} and Fe^{2+} peaks were separated by the Gaussian fitting method. As shown in Fig. S7 A, the Fe 2p3/2 region are fitted into two spin orbit doublets with the binding energy at 710.9 ± 0.2 and 712.0 ± 0.2 eV assigned to the presence of Fe^{2+} and Fe^{3+} cations, respectively. Compared with the Fe 3p region of un-doped $FeVO_4$-nanoporous sample, the intensity of Fe 3p peaks and its satellite peaks assigned to the oxidation states of Fe^{3+} in the Fe^{3+} self-doped $FeVO_4$ are significantly increased. In contrast, the intensity of Fe^{2+} in the 3p peaks and satellite peaks intensity are higher than the un-doped $FeVO_4$ spectra. Additionally, the shifting phenomena could also be evidently observed in the O 1s XPS spectra (Fig. S7 B), which may reveal the influence of the different valence state of Fe on the Fe^{3+} or Fe^{2+} self-doping surfaces.

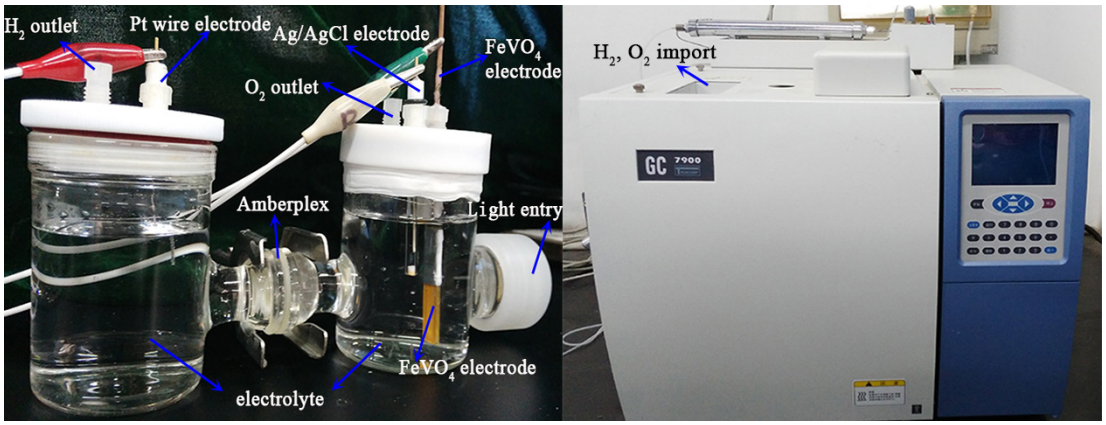

Fig. S9 Digital photo of the self-made H_2 generation and collection system.

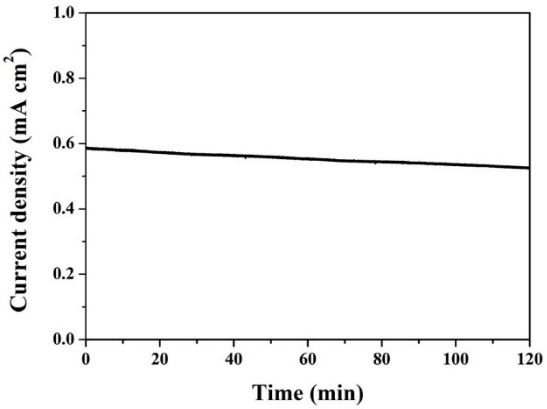

Fig. S10 Water oxidation photocurrent *i-t* curve for the Fe^{3+} self-doped $FeVO_4$-nanoporous photoanode measured up to 150 min at 0.8 V at 1.0 V (*vs.* Ag/AgCl) constant potential (also used for the calculation of Faradaic efficiencies of H_2 and O_2 in Fig. 3D).

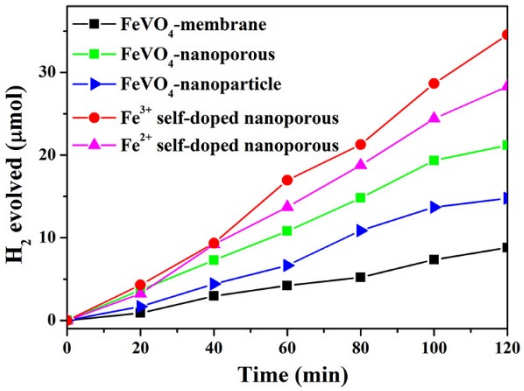

Fig. S11 Detection of H_2 evolution of the $FeVO_4$-membrane, $FeVO_4$-nanoprous, $FeVO_4$-nanoparticles, Fe^{3+} self-doped $FeVO_4$-nanoporous and Fe^{2+} self-doped $FeVO_4$-nanoporous photoanodes in electrolyte of 0.2 mol L^{-1} Na_2SO_4 and 0.1 mol L^{-1} phosphate buffer solution (pH 7.0). Measured at 0.8 V (vs. Ag/AgCl). The results show that the continuous H_2 are produced when solar light irradiation and applying bias voltage (0.8 V vs. Ag/AgCl). More specifically, the H_2 generation amounts over Fe^{3+} and Fe^{2+} doped $FeVO_4$ photoanodes reach up to 35 and 28 μmol after 120 min, respectively, which are higher than that of un-doped samples. Furthermore, the H_2 generation rate of Fe^{3+} and Fe^{2+} doped photoanodes is nearly about 1.7 times and 1.2 times higher than that of the un-doped photoanodes, which is consistent with the photocurrent comparisons of the Fe^{3+} and Fe^{2+} self-doped (1.06 mA/cm^2 and 0.79 mA/cm^2 at 1.0 V (*vs.* Ag/AgCl)) and un-doped $FeVO_4$ photoanodes (0.64 mA cm^{-2}).

Table S3. Results obtained for iron content in the $FeVO_4$ samples assayed by the *o*-phenanthroline colorimetric method.

samples	total Fe		Fe^{2+}		Fe^{3+}	
	concentration (mg/mL)	relative content (%)	concentration (mg/mL)	relative content (%)	concentration (mg/mL)	relative content (%)
$FeVO_4$-nanoporous	0.972	100	0.116	11.93	0.856	88.07

Fe^{3+} self-doping $FeVO_4$-nanoporous	0.954	100	0.032	3.35	0.922	96.65
Fe^{2+} self-doping $FeVO_4$-nanoporous	0.978	100	0.184	18.81	0.794	81.19

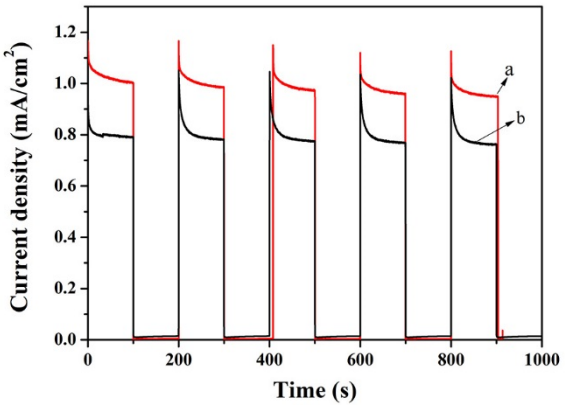

Fig. S12 Chronoamperometric *i-t* curves at 1.0 V (vs. Ag/AgCl) of the (a) Fe^{3+} self-doped $FeVO_4$-nanoporous and (b) Fe^{2+} self-doped $FeVO_4$-nanoporous photoanodes in electrolyte of 0.2 mol L^{-1} Na_2SO_4 and 0.1 mol L^{-1} phosphate buffer solution (pH 7.0). The transient photocurrent density of Fe^{3+} and Fe^{2+} doped photoanodes could reach up to 1.06 mA/cm^2 and 0.79 mA/cm^2 and maintain for 1000s without showing any sign of decay.

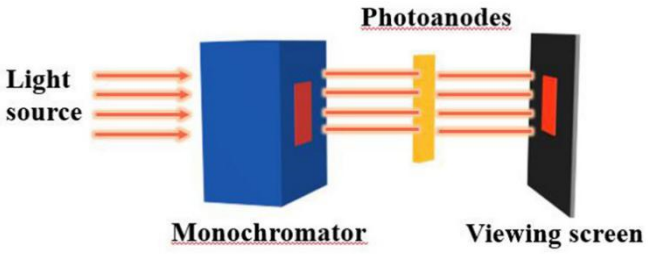

Fig. S13 Optical system diagram of the monochromatic light transmission

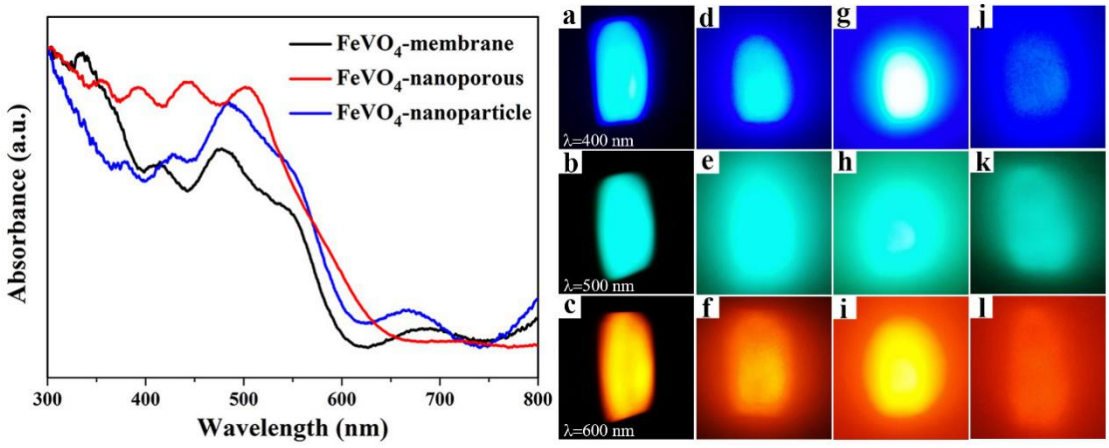

Fig. S14 Absorption spectra of $FeVO_4$-membrane, $FeVO_4$-nanoporous and $FeVO_4$-nanaoparticle photoanodes. The transmission phenomena of monochromatic lights with different wavelengths: without photoanodes (a, b, c) $FeVO_4$-membrane (d, e, f), $FeVO_4$-nanoporous (g, h, i) and $FeVO_4$-nanaoparticle (j, k, l) photoanodes. It has been confirmed that the porous film could enhance the light harvesting due to light diffraction within the nanopores by increasing the optical path length of light, especially in the wavelength range corresponding to the band edge.

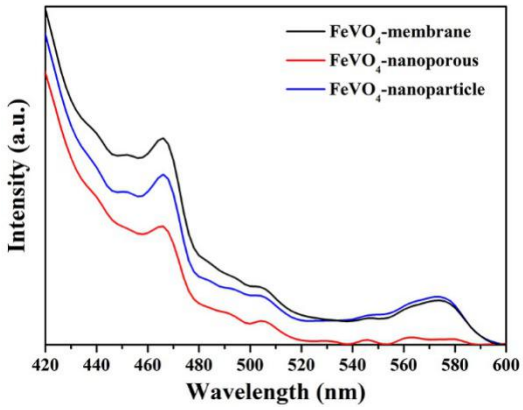

Fig. S15 PL spectra of the $FeVO_4$ photoanodes excited at 350 nm. The PL spectrum indicates a strong peak at 470 nm, which corresponds to the high-level transition in $FeVO_4$[5, 6]. Among the different samples, $FeVO_4$-nanoporous, which has the lowest intensity in that particular region, demonstrates that the recombination process can be effectively restrained in the nanoporous $FeVO_4$. Therefore, $FeVO_4$-nanoporous photoanodes is very effective for separating the photo-generated charge carriers, which in turns triggers the charge transfer process at a faster rate than the membrane and nanoparticle semiconductor films.

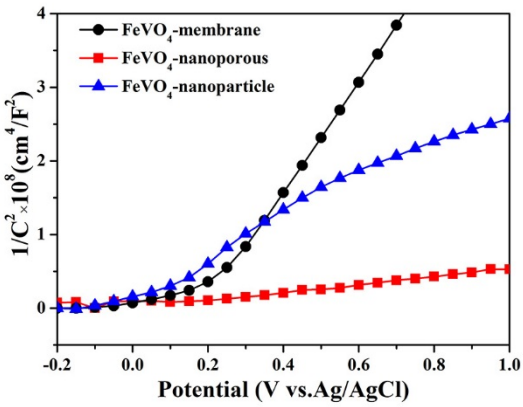

Fig. S16 Mott–Schottky plots for $FeVO_4$-membrane, $FeVO_4$-nanoporous and $FeVO_4$-nanoparticle photoanodes at 1 kHz in the dark. The $FeVO_4$-nanoporous photoanode showed a substantially smaller slope of the Mott–Schottky plot than the other materials, suggesting an increase of donor density due to the nanoporous structure, which effectively promotes the electrical conductivity and charge transport.

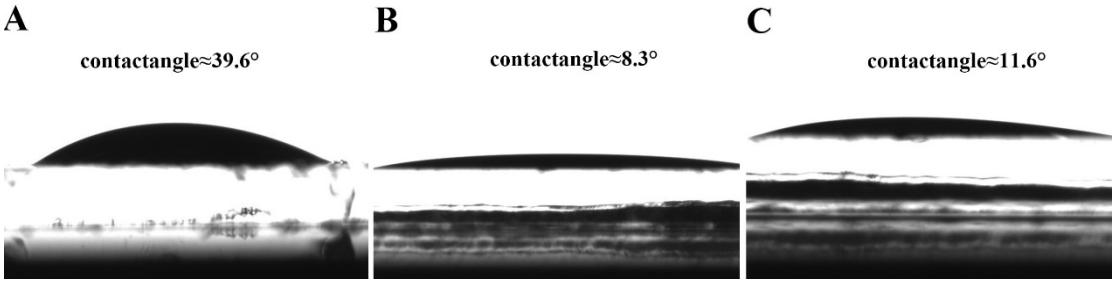

Fig. S17 The contact angle images of (A) $FeVO_4$-membrane, (B) $FeVO_4$-nanoporous, (C) $FeVO_4$-nanoparticle on the surface of FTO substrates. Compared with the contact angle of $FeVO_4$-membrane (39.6°) and $FeVO_4$-nanoparticle (11.6°), the $FeVO_4$-nanoprous film exhibits a decrease in contact angle of 8.3°, indicating that $FeVO_4$-nanoprous film has excellent hydrophobicity.

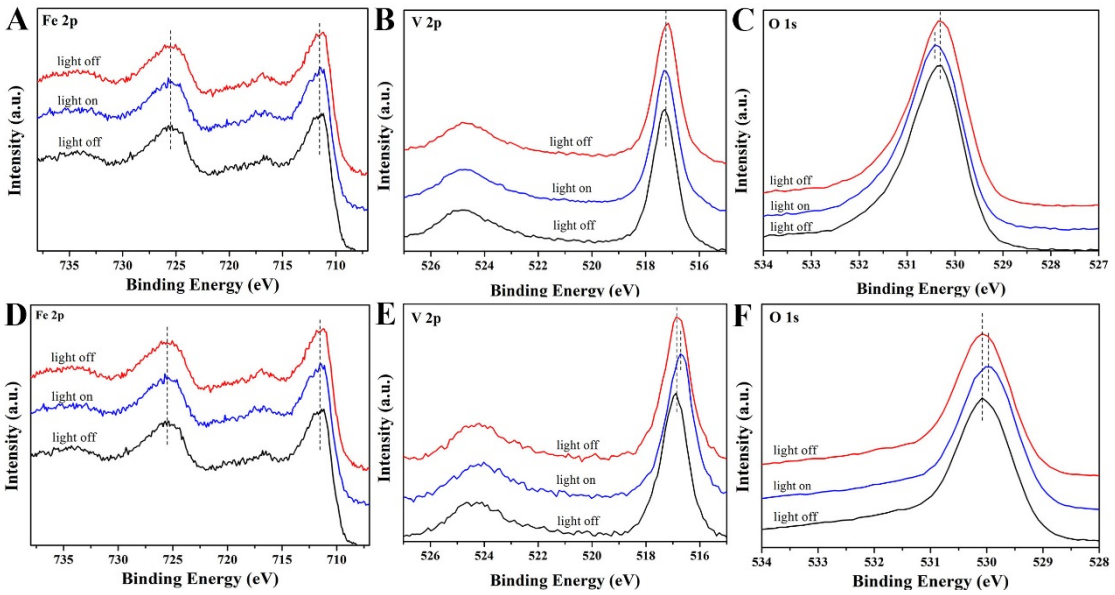

Fig. S18 The SIXPS spectra for Fe 2p, V 2p and O 1s of (A-C) Fe^{3+} self-doped $FeVO_4$-nanoporous photoanode and (D-F) Fe^{2+} self-doped $FeVO_4$-nanoporous photoanode, respectively.

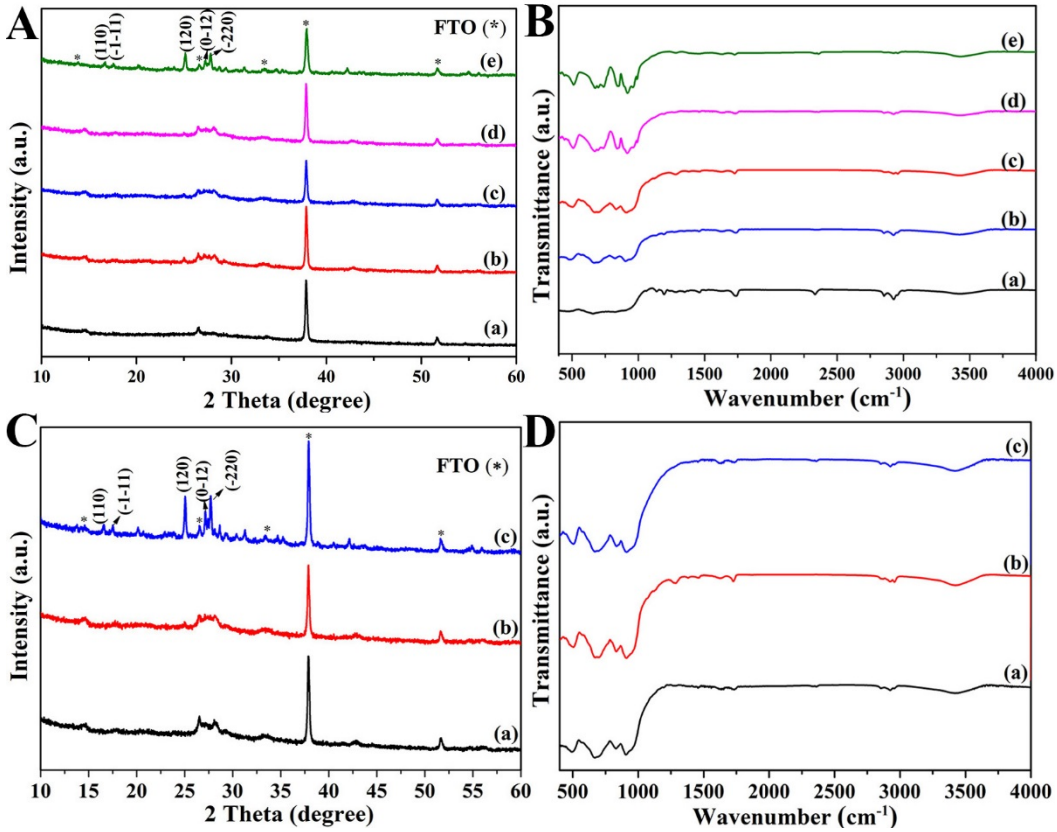

Fig. S19 (A) XRD patterns and (B) IR spectra of $FeVO_4$ photoanodes annealed at different temperatures: (a) 400 °C, (b) 450 °C, (c) 500 °C, (d) 550 °C,(e) 600 °C for 2.5 h; (C)The XRD patterns and (D) IR spectra of $FeVO_4$ photoanodes annealed at: (a) 1.0 h, (b) 2.5 h and (c) 6.0 h. The IR spectra were conducted using powder samples that were scraped from the films.

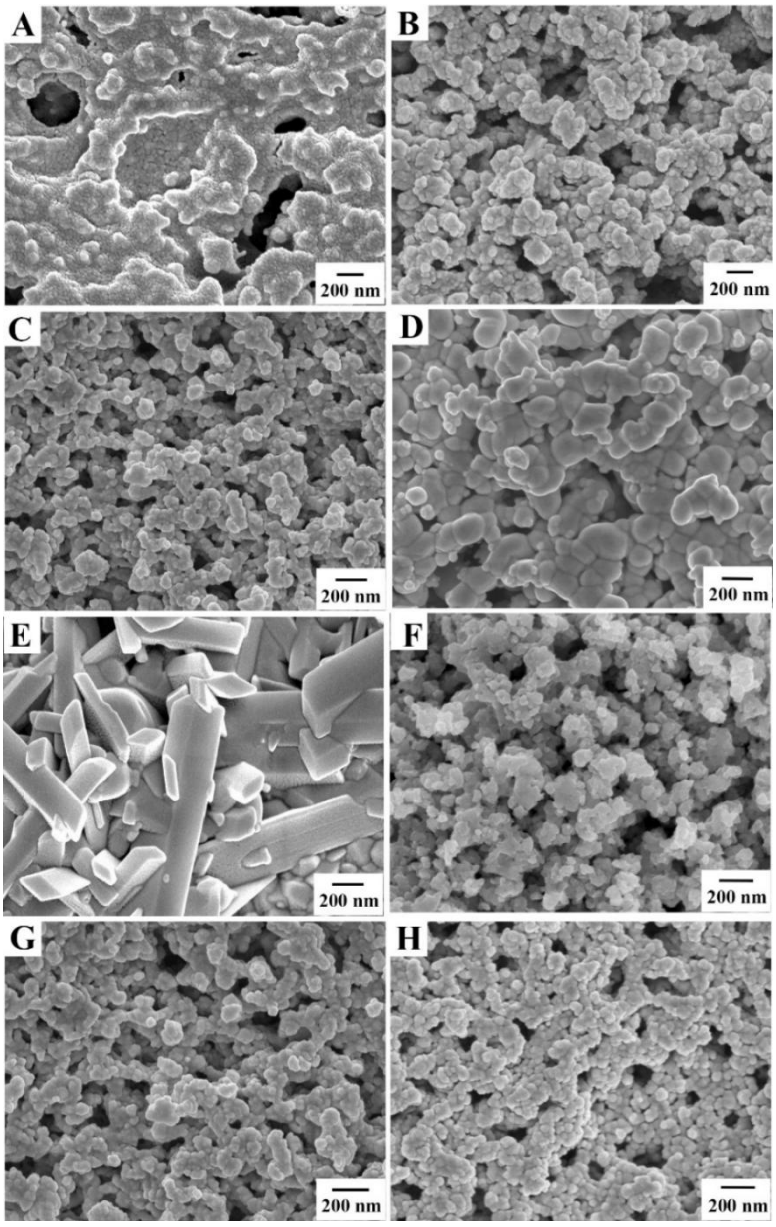

Fig. S20 The FE-SEM images of $FeVO_4$ photoanodes annealed at different temperatures: (A) 400 °C, (B) 450 °C, (C) 500 °C, (D) 550 °C, (E) 600 °C for 2.5 h, and $FeVO_4$ photoanodes annealed at 500 °C for (F) 1.0 h, (G) 2.5 h and (H) 6.0 h.

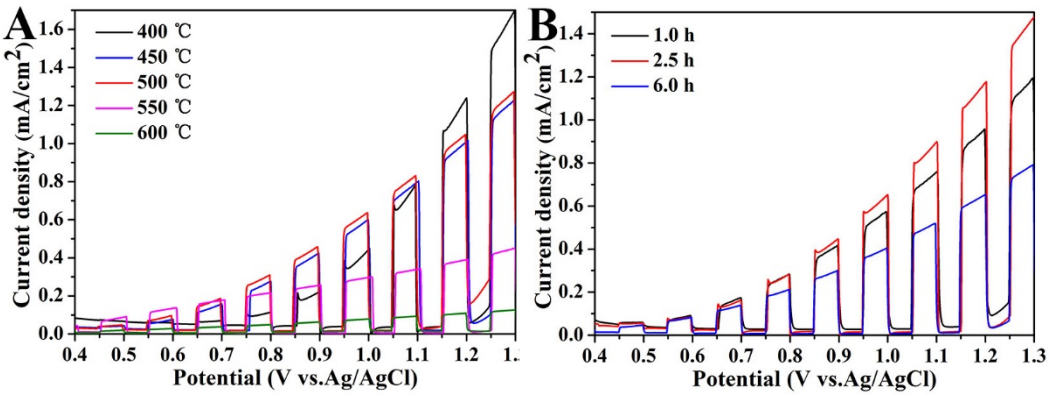

Fig. S21 The LSVs of (A) $FeVO_4$-nanoporous photoanodes annealed at different temperatures (400 °C, 450 °C, 500 °C, 550 °C and 600 °C) for 2.5h, and (B) $FeVO_4$ photoanodes annealed at 500 °C for different times (1.0 h, 2.5 h and 6.0 h). Measurements were conducted in electrolyte of 0.2 mol L^{-1} Na_2SO_4 and 0.1 mol L^{-1} phosphate buffer solution (pH 7.0). The scan rate was 10 mV s^{-1}.

Effect of the annealing temperature and time on $FeVO_4$-nanoporous photoanodes

Variation of annealing temperatures between 400 and 600 °C, and annealing times from 1 to 6 h have influence on the morphology structure and PEC activity of $FeVO_4$. The X-ray diffraction (XRD) patterns of preparing sample photoelectrodes (Fig. S19A) indicate a clear increase in crystallinity when the $FeVO_4$ are annealed at higher temperatures, in particular those annealed above 450 °C (Fig. S19A). For samples annealing above 600 °C, the crystallinity increases markedly and the resolved peaks can be assigned the orthorhombic phase of $FeVO_4$ (JCPDS 038-1372) (Fig. S19A). Infrared spectra (IR) for samples annealed in air are shown in Fig. S19B. The spectra resulting from samples annealed at 400 °C display broad, ill-defined features below 1000 cm^{-1}, typical of amorphous material (Fig. S19B). In a similar trend to that observed in the XRD data, the IR spectra show sharper, better-defined bands as the annealing temperature increases (Fig. S19B), corresponding to the crystalline structure of $FeVO_4$. Similar to the above analysis, when the time varied from 1 to 6 h, the crystalline nature of $FeVO_4$ can be observed from the increased sharpness and the number of XRD and IR peaks (Fig. S19C and D).

Meanwhile, the FE-SEM consolidated the interpretation of the XRD and IR analysis (Fig. S20). In Fig. S20A, the surfaces are found to be covered with agglomerated particles at 400 °C. As the annealing temperature increases, the well-defined particles are formed and the size of the particles have become larger (Fig. S20A-E). More specially, the more porous constructed by

numerous inter-crossed nanoparticles of the film are formed at 500 °C (Fig. S20C). Additionally, when the annealing time varied from 1 to 6 h, the porous nature of the $FeVO_4$ film have not a significant change (Fig. S20F-H).

A series of electrodes were prepared by varied annealing temperatures between 400 and 600 °C, and annealing times from 1 to 6 h. The chopped LSVs were recorded upon exposure of the electrodes under the simulated solar light irradiation (AM 1.5G, 100 mW cm^{-2}) (Fig. S21). It can be seen that photocurrent increases to 0.64 mA cm^{-2} at 1.0 V (vs. Ag/AgCl) for the electrode annealed at 500 °C for 2.5 h. Therefore, 500 °C for 2.5 h are chosen as the optimal synthesis conditions for all experiments.

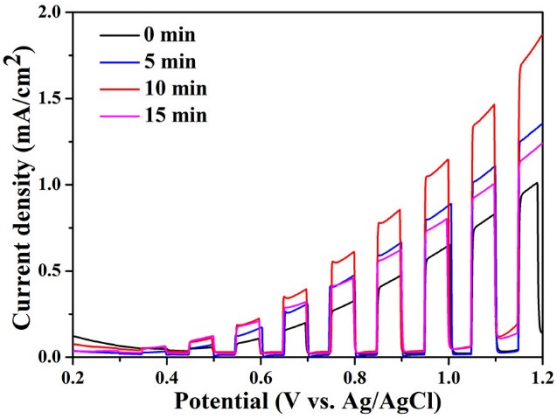

Fig. S22 The LSVs of Fe^{3+} self-doped photoanodes by H_2O_2 oxidation (30 wt %) for 0 min, 5 min, 10 min and 15 min, respectively. Measurements were conducted in electrolyte of 0.2 mol L^{-1} Na_2SO_4 and 0.1 mol L^{-1} phosphate buffer solution (pH 7.0). The scan rate was 10 mV s^{-1}.

Effect of oxidation time of Fe^{3+} self-doped $FeVO_4$ photoanode

The different immersing time of $FeVO_4$-nanoprous into H_2O_2 (30%) are used to prepare Fe^{3+} self-doped $FeVO_4$-nanoprous photoanodes and its PEC properties are shown in Fig. S22. In comparison with un-doped $FeVO_4$-nanoprous photoanodes, all Fe^{3+} self-doped photoanodes exhibit improved photocurrents at higher applied potential. When immersing into H_2O_2 for 10 min, the photocurrent density of Fe^{3+} self-doped $FeVO_4$-nanoprous photoanodes reaches 1.14 mA cm^{-2}, which is increased 1.7 times compared to that of the undoped $FeVO_4$-nanoprous (Fig. S22).

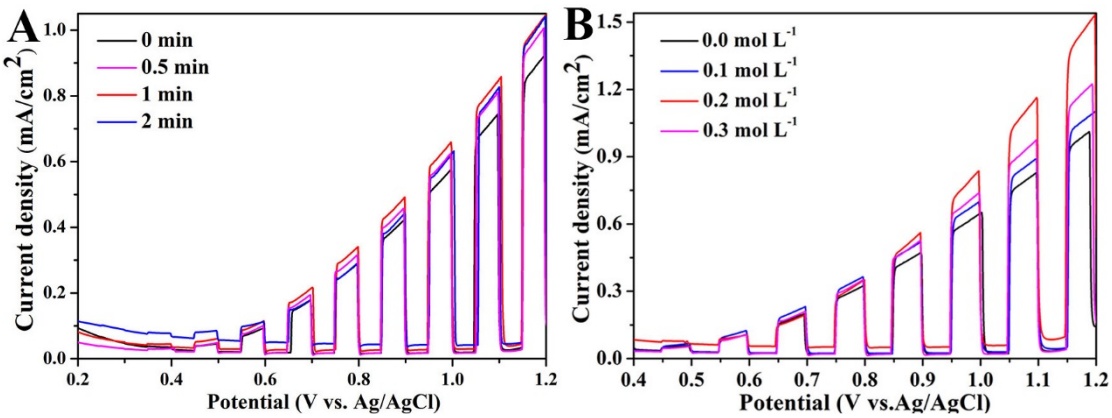

Fig. S23. The LSVs of Fe^{2+} self-doped photoanodes prepared by (A) 0.1 mol L^{-1} $NaBH_4$ for 0 min, 0.5 min, 1 min and 2 min, respectively; (B) the different concentrations of $NaBH_4$ with 0.0 mol L^{-1}, 0.1 mol L^{-1}, 0.2 mol L^{-1} and 0.3 mol L^{-1} for 1 min. Measurements were conducted in electrolyte of 0.2 mol L^{-1} Na_2SO_4 and 0.1 mol L^{-1} phosphate buffer solution (pH 7.0). The scan rate was 10 mV s^{-1}.

Effect of the reduction time and concentration of Fe^{2+} self-doped $FeVO_4$-nanoporous photoanode

The Fe^{2+} self-doped $FeVO_4$ photoanode was obtained by reducing of $FeVO_4$-nanoprous with freshly made $NaBH_4$ solution. The PEC performances of Fe^{2+} self-doped $FeVO_4$-nanoprous prepared by different reaction time and different concentrations of $NaBH_4$ are presented in Fig. S23. In comparison with pure $FeVO_4$-nanoprous, all Fe^{2+} self-doped photoanodes exhibit improved photocurrents at higher applied potentials. When a 0.2 mol L^{-1} $NaBH_4$ reduced for 1 min, the improvement of the Fe^{2+} self-doped $FeVO_4$ photoanodes is most remarkable photocurrent from 0.64 mA cm^{-2} to 0.84 mA cm^{-2} at 1.0 V (vs. Ag/AgCl).

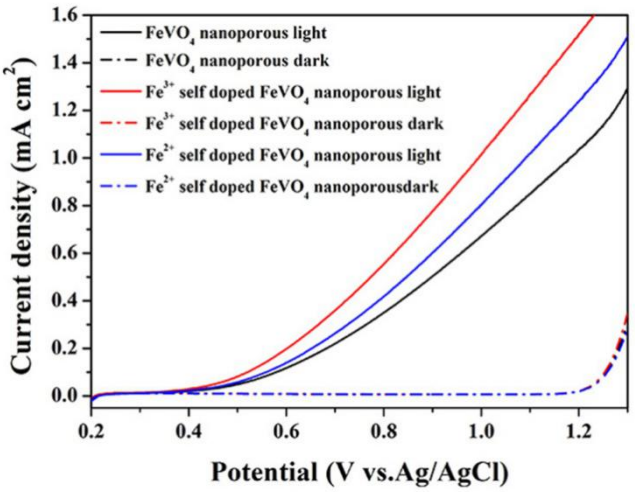

Figure S24. Current–potential curves of different $FeVO_4$ electrodes measured under simulated AM1.5G illumination and in the dark (dotted lines). Measurements were conducted in electrolyte of 0.2 mol L^{-1} Na_2SO_4 and 0.1 mol L^{-1} phosphate buffer solution (pH 7.0). Dark current is shown as dashed lines. Scan rate: 10 mV s^{-1}.

References and Notes

1. J. Y. Kim, D. H. Youn, K. Kang and J. S. Lee, *Angew. Chem. Int. Ed.*, 2016, **55**, 10854-10858
2. H. Tamura, K. Goto, T. Yotsuyanagi and M. Nagayama, *Talanta*, 1974, **21**, 314-318.
3. C. Jiang, Z. Gao, H. Qu, J. Li, X. Wang, P. Li and H. Liu, *J. Hazard. Mater.*, 2013, **250**, 76-81.
4. T. Yamashita and P. Hayes, *Appl. Surf. Sci.*, 2008, **254**, 2441-2449.
5. H. Mandal, S. Shyamal, P. Hajra, A. Bera, D. Sariket, S. Kundu and C. Bhattacharya, *Rsc. Adv.*, 2016, **6**, 4992-4999.

6. X. Liu, Y. Kang and D. Luo, *Mater. Lett.*, 2016, **185**, 189-192.